JOURNAL OF MAGNETIC RESONANCE **128,** 228–232 (1997)
ARTICLE NO. MN971235

COMMUNICATION

Two-Dimensional *ct*-HC(C)H-COSY for Resonance Assignments of Smaller ^{13}C-Labeled Biomolecules

Thomas Szyperski, César Fernández, and Kurt Wüthrich

Institut für Molekularbiologie und Biophysik, Eidgenössische Technische Hochschule-Hönggerberg, CH-8093 Zürich, Switzerland

Received May 2, 1997; revised July 30, 1997

Key Words: **NMR assignments, ^{13}C labeling, reduced-dimensionality, projected NMR experiments.**

This Communication describes the reduced-dimensionality (*1–5*) 2D *ct*-HC(C)H-COSY experiment (the underlined ^{1}H and ^{13}C spins are sampled simultaneously (*2*)), which provides high resolution for indirectly measured ^{1}H and ^{13}C chemical shifts even with short recording times. Two-dimensional *ct*-HC(C)H-COSY derives from 3D *ct*-HC(C)H-COSY (*6*) and 2D *ct*-(H)C(C)H-COSY (*7*). In the latter experiment the indirect proton dimension is omitted and hence the introduction of a constant-time (ct) ^{13}C evolution period, which may extend over one or several $^1J(^{13}\mathrm{C}, ^{13}\mathrm{C})$ dephasing/rephasing cycles (*8, 9*), enables the use of long $t_{1,\max}(^{13}\mathrm{C})$ values and concomitant high resolution in the ^{13}C dimension. In the present implementation of 2D *ct*-HC(C)H-COSY, use of the high resolution attainable with 2D *ct*-(H)C(C)H-COSY is combined with the potentialities of 3D *ct*-HC(C)H-COSY (*6*).

The pulse scheme of 2D *ct*-HC(C)H-COSY (Fig. 1) shows that magnetization is transferred in the linear ''out-and-stay'' fashion (*10*) as described previously for the parent 3D HC(C)H-COSY experiment (*6*), of which the new experiment is a ''projection'' (*1–5*). The experiment thus correlates the resonances of vicinal proton pairs with the chemical shift of the ^{13}C nucleus attached to one of the protons (Fig. 2), or those of geminal proton pairs with the directly bound ^{13}C atom. The evolution of the chemical shifts in the projected ^{1}H dimension gives rise to a cosine modulation of the transfer amplitude (*1, 2*), so that the magnetization that was initially excited on ^{1}H generates peak doublets. Because the refocusing delay of the first INEPT step (τ_2 in Fig. 1) is set to a compromise value to ensure acceptable simultaneous magnetization transfer from ^{1}H to methine, methylene, and methyl carbons (*11*), a substantial fraction of the single-quantum coherence originating from ^{13}C steady-state magnetization is not dephased at the end of this delay. In the parent 3D experiment (*6*) this coherence is discarded by axial peak suppression, but in projected experiments it can be exploited to yield peaks located in the center of the doublets (*5*). These central peaks provide unambiguous identification of multiple peak doublets with identical $^1\mathrm{H}(\omega_2)$ chemical shifts and peak intensities, and enable straightforward improvement of the spectra by symmetrization (*5*). Moreover, the ^{13}C steady-state magnetization of quaternary carbons directly attached to a CH_n moiety, e.g., the γ carbon of tyrosine, yields cross peaks at the chemical shifts of the quaternary carbons along ω_1, which are not accessible by the parent 3D HC(C)H-COSY experiment.

^{13}C frequency labeling is achieved during a constant-time period (*6*), which can optionally be extended by multiples of $\delta = 1/\{2\,^1J(^{13}\mathrm{C}, ^{13}\mathrm{C})\}$ in order to attain larger $t_{1,\max}(^{13}\mathrm{C})$ values. This is of practical interest for molecules with low molecular weight and long $T_2(^{13}\mathrm{C})$ relaxation times, for example, ^{13}C-labeled oligosaccharides (*7*). Following the product operator descriptions of 3D *ct*-HC(C)H-COSY (*6*) and 2D *ct*-[^{13}C, ^{1}H]-HSQC (*8, 9*), and the previously introduced simultaneous acquisition of multiplets and central peaks in projected NMR experiments (*5*), the density matrix σ describing detectable magnetization at the beginning of the acquisition time is given by

$$\begin{aligned}\sigma \sim\ & (\mathbf{1})^n I_x \sin(\pi J_{\mathrm{CH}}\tau_2)\sin(\pi J_{\mathrm{CH}}\tau_1)\\ & \times \sin[\pi J_{\mathrm{CC}}(\tau_3 + i\cdot\delta)]\cos^l(\pi J_{\mathrm{CH}}\tau_2)\\ & \times \sin(\pi J_{\mathrm{CC}}\tau_3)\cos^n(\pi J_{\mathrm{CC}}\tau_3)\cos^m(\pi J_{\mathrm{CC}}\tau_3)\\ & \times \{R_{\mathrm{H}}\sin(\pi J_{\mathrm{CH}}\tau_1)\sin(\pi J_{\mathrm{CH}}\tau_2)\cos^k(\pi J_{\mathrm{CH}}\tau_2)\\ & \quad \times \cos[\kappa\Omega(^1\mathrm{H}_1)t_1]\cos[\Omega(^{13}\mathrm{C}_1)t_1]\\ & \quad + R_{\mathrm{C}}\cos^{k+1}(\pi J_{\mathrm{CH}}\tau_2)\sin[\Omega(^{13}\mathrm{C}_1)t_1]\},\end{aligned} \qquad [1]$$

with

$$R_{\mathrm{H}} = 1 - \exp\{-T_{\mathrm{rel}}/T_1(^1\mathrm{H})\} \quad \text{and}$$
$$R_{\mathrm{C}} = \gamma(^{13}\mathrm{C})/\gamma(^1\mathrm{H})[1 - \exp\{-T_{\mathrm{rel}}/T_1(^{13}\mathrm{C})\}].$$

1090-7807/97 $25.00

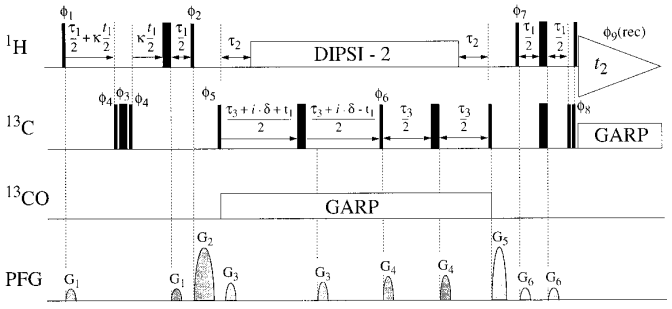

FIG. 1. Experimental scheme for 2D *ct*-HC(C)H-COSY and parameters used to record the spectra in Figs. 3–5. Rectangular 90° and 180° pulses are indicated by thin and thick black bars, respectively, and phases are indicated above the pulses (where no phase is given, the pulse is applied along x). Ninety degree pulse lengths of 9.5 μs and 12 μs were used for ^{1}H and ^{13}C, respectively, and the 180° pulses were applied with the same power. For ^{1}H the carrier was placed at 2.90 ppm, and for aliphatic and carbonyl ^{13}C at 34 ppm and 171 ppm, respectively. ^{13}C decoupling during $t_1(^1\mathrm{H})$ is achieved with a $(90_y-180_x-90_y)$ composite pulse (*28*). The $^{13}\mathrm{C}(90_x-90_{\phi 9})$ pulse pair immediately before acquisition serves to reduce the intensity of modulation sidebands originating from incompletely refocused ^{1}H magnetization (*29*). The scaling factor for chemical shift evolution of ^{1}H is given by κ. A DIPSI-2 sequence (*30*) (RF = 2.5 kHz) is used to decouple ^{1}H during the heteronuclear magnetization transfers, a GARP sequence (*31*) (RF = 2.5 kHz) to decouple ^{13}C during the proton detection, and a GARP sequence (RF = 0.6 kHz) for ^{13}CO composite pulse decoupling. Phase cycling: $\phi_1 = x$; $\phi_2 = y$; $\phi_3 = x, -x$; $\phi_4 = y, -y$; $\phi_5 = x$; $\phi_6 = x, -x$; $\phi_7 = x, -x$; $\phi_8 = x, -x$; ϕ_9 (receiver) $= x, -x$. Quadrature detection in $t_1(^{13}\mathrm{C})$ was accomplished by alternating the phase ϕ_5 according to States–TPPI (*32*). The apparent ^{1}H carrier position was shifted to 6.37 ppm by incrementing ϕ_1 in 45° steps according to TPPI (*15*). The delays had the following values (*6*): $\tau_1 = 3.4$ ms, tuned approximately to $0.5/J_{\mathrm{CH}}$; $\tau_2 = 2.1$ ms, tuned to $0.3/J_{\mathrm{CH}}$; $\tau_3 = 7.4$ ms, tuned approximately to $0.25/J_{\mathrm{CC}}$. For $i = 2$, $\delta = 26.6$ ms when tuned to $1/J_{\mathrm{CC}}$. The durations and amplitudes of the sine bell-shaped pulse field gradients (PFG) are 400 μs and 10 G/cm for G_1 and G_6, 2 ms and 50 G/cm for G_2, 400 μs and 15 G/cm for G_3, 400 μs and 20 G/cm for G_4, and 1 ms and 50 G/cm for G_5. The recovery delays after G_2 and G_5 were set to 1 ms. Two data sets were recorded with $\phi_2 = y$ and $\phi_2 = -y$, respectively, for simultaneous acquisition of the peak doublets, which are obtained in the difference spectrum, and the central peaks, which are obtained in the sum spectrum (see text).

The number of increments δ added to τ_3 (Fig. 1) is given by i, I is the spin operator of the detected proton H_2 (Fig. 2), J_{CC} and J_{CH} are the one-bond carbon–carbon and carbon–proton couplings, n and m indicate the number of passive J_{CC} couplings for the carbon atoms C_1 and C_2 (Fig. 2), k and l indicate the number of passive J_{CH} couplings for the protons H_1 and H_2 (Fig. 2), κ denotes the scaling factor for chemical shifts in the projected dimension (*3*), $\Omega(X)$, $T_1(X)$ and $\gamma(X)$ are the chemical shift, the longitudinal relaxation time, and the gyromagnetic ratio of nucleus X, and T_{rel} denotes the relaxation delay between scans. The factor $(-\mathbf{1})^n$ must be taken into account for $i = 1, 2, 5, 6\cdots$ (variant I), but not for $i = 0, 3, 4, 7, 8\cdots$ (variant II). In variant I the sign of the peaks from carbons coupled to an odd number of ^{13}C spins is thus opposite to that for a carbon with an even number of $^{13}\mathrm{C}-{}^{13}\mathrm{C}$ couplings, but the same sign is obtained for all peaks in variant II (*8, 9*). With quadrature detection of ^{13}C, the first term in Eq. [1] gives rise to a peak doublet located at $\omega_2(^1\mathrm{H}_2)$, with peaks at $\omega_1(^{13}\mathrm{C}_1) \pm \Delta\omega_1(^1\mathrm{H}_1)$, and the second term yields the corresponding central peak at $\omega_2(^1\mathrm{H}_2)/\omega_1(^{13}\mathrm{C}_1)$ (see Fig. 2 for the atom numeration). Since the central peaks are dispersive when the doublets are phased absorptive, we recommend to record two data sets by inverting the phase ϕ_2 in Fig. 1 (*5*). The difference of the two data sets yields the doublets, while the sum contains the central peaks, and the two subspectra can be phased separately to obtain absorptive peaks.

Pulsed field gradients (PFG) were used for coherence pathway rejection (*12, 13*). To minimize off-resonance effects we placed the ^{1}H carrier in the center of the spectral range and performed time-proportional phase incrementation (TPPI) (*4, 14, 15*) on ϕ_1, thereby shifting the apparent carrier position to 6.37 ppm at the downfield edge of the ^{1}H resonances (Fig. 1). For the aliphatic side chains of ^{13}C-labeled polypeptides the delays τ_1 and τ_3 (Fig. 1) were tuned with $^1J_{\mathrm{CH}} = 140$ Hz and $^1J_{\mathrm{CC}} = 37$ Hz. For other chemical structures the delays must be adapted according to the relations given in the legend to Fig. 1.

As a first illustration we acquired a variant II 2D *ct*-HC(C)H-COSY experiment with $i = 0$ for the uniformly ^{13}C-labeled cyclic undecapeptide cyclosporin A (CsA), with a constant time delay of 6.6 ms duration. Figure 3, A and B, shows contour plots taken from the resulting subspectra. The peak pairs of the $\mathrm{H}^\alpha-\mathrm{H}^\alpha$ transfer (corresponding to a backtransfer of magnetization, $\mathrm{H}_2 \rightarrow \mathrm{C}_2 \rightarrow \mathrm{H}_2$ in Fig. 2) and the $\mathrm{H}^\beta-\mathrm{H}^\alpha$ transfer ($\mathrm{H}_1 \rightarrow \mathrm{C}_1 \rightarrow \mathrm{C}_2 \rightarrow \mathrm{H}_2$ in Fig. 2) are observed in Fig. 3B at $\omega_2(^1\mathrm{H}^\alpha)$, where they are centered about the peaks at $\omega_1(^{13}\mathrm{C}^\alpha)$ and $\omega_1(^{13}\mathrm{C}^\beta)$, respectively. The in-phase splittings yield the chemical shifts of protons attached to the carbon for which the chemical shift is encoded in the central peak (Fig. 3A). Since both subspectra are derived from the same experiment, which ensures accurate relative positioning of the singlet and doublet peaks, the doublets in Fig. 3B can be neatly separated by symmetrization (*4, 5, 15, 16*) relative to the individual central peaks (Fig. 4).

As a second example, which emphasizes the high resolution that can be obtained with 2D *ct*-HC(C)H-COSY experiments, variant I with $i = 2$ and $t_{1,\max} = 33.2$ ms was recorded for CsA (Figs. 3C and 5). Signals from carbon atoms with one or three passive J_{CC} couplings (for example, C^α-MeLeu

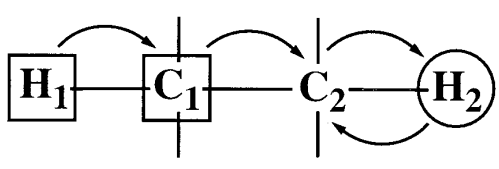

FIG. 2. Magnetization transfer pathway of the 2D *ct*-HC(C)H-COSY experiment. The two square boxes indicate that the chemical shifts of these two nuclei are observed in a common dimension. The arrows represent HSQC-type transfers of magnetization, and the circle indicates that the magnetization is detected on the proton H_2.

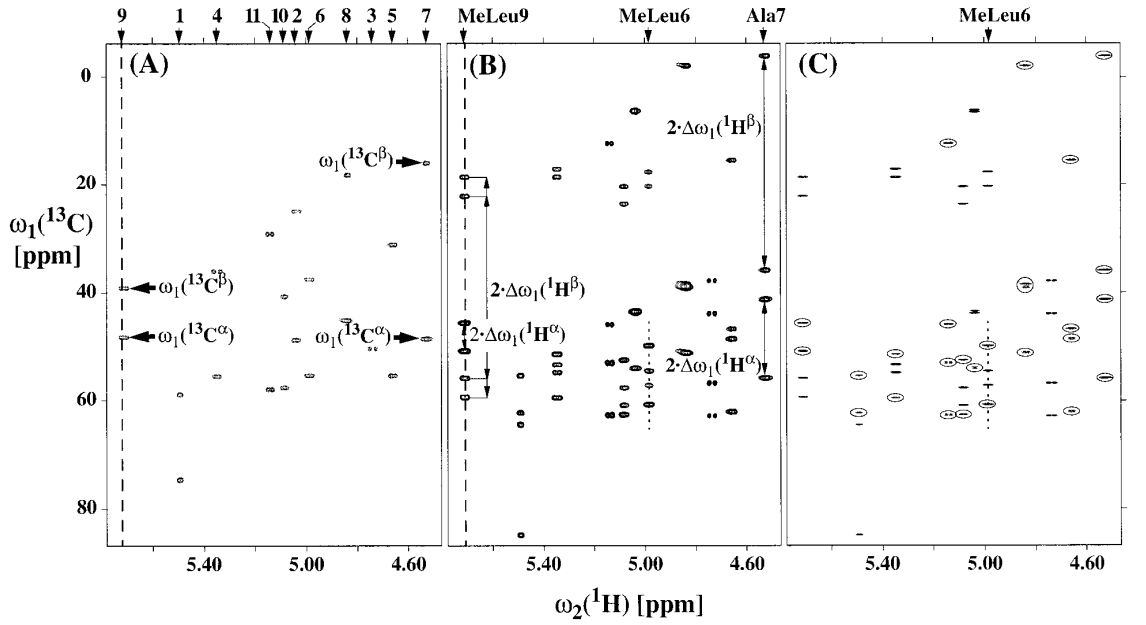

FIG. 3. Contour plots showing 2D *ct*-HC(C)H-COSY spectra recorded with acquisition of central peaks (*5*), which contain the signals detected on the α protons of uniformly ^{13}C-labeled CsA dissolved in 100% $CDCl_3$ (T = 23°C, concentration 10 mM). CsA is *cyclo*(–MeBmt1–Abu2–Sar3–MeLeu4–Val5–MeLeu6–Ala7–D–Ala8–MeLeu9–MeLeu10–MeVal11–), with MeBmt = (2S, 3R, 4R, 6E)-3-hydroxy-4-methyl-2-(methylamino)oct-6-enoic acid, Sar = sarcosine, MeLeu = *N*-methylleucine, MeVal = *N*-methylvaline, and Abu = aminobutyric acid. (A) Sum subspectrum showing the central peaks obtained from the sum of the two data sets recorded with a ϕ_2 phase shift of 180° and i = 0, so that δ = 0 ms (Eq. [1] and Fig. 1). The peak positions along ω_1 are at $\omega_1(^{13}C^{\alpha})$ and $\omega_1(^{13}C^{\beta})$. The assignments of the peaks to the individual residues (*17*) are given by the sequence numbers at the top of the spectrum. For residues Ala7 and MeLeu9 the $^{13}C^{\alpha}$ and $^{13}C^{\beta}$ peaks are individually identified. (B) Difference subspectrum containing the doublets corresponding to the peaks in (A). We used κ = 1 (Fig. 1), so that the peak positions are at $\omega_1(^{13}C^{\alpha}) \pm \Delta\omega_1(^1H^{\alpha})$ and $\omega_1(^{13}C^{\beta}) \pm \Delta\omega_1(^1H^{\beta})$. The in-phase splittings measured on the ^{13}C chemical shift scale in ppm, $2\cdot\Delta\omega_1(^1H)$, are equal to $2\cdot\delta\omega(^1H)\cdot[\gamma(^1H)/\gamma(^{13}C)]$, where $\delta\omega(^1H)$ denotes the chemical difference in ppm with respect to the ^{1}H carrier position at 6.37 ppm. The splittings are identified by solid arrows for the residues Ala7 and MeLeu9, which indicates how the following chemical shifts relative to TMS were extracted: $\omega_1(^1H^{\alpha}$, Ala7) = 4.52 ppm, $\omega_1(^{13}C^{\alpha}$, Ala7) = 48.69 ppm, $\omega_1(^1H^{\beta}$, Ala7) = 1.37 ppm, $\omega_1(^{13}C^{\beta}$, Ala7) = 16.07 ppm, $\omega_1(^1H^{\alpha}$, MeLeu9) = 5.70 ppm, $\omega_1(^{13}C^{\alpha}$, MeLeu9) = 48.30 ppm, $\omega_1(^1H^{\beta 1}$, MeLeu9) = 1.25 ppm, $\omega_1(^1H^{\beta 2}$, MeLeu9) = 2.13 ppm, $\omega_1(^{13}C^{\beta}$, MeLeu9) = 39.04 ppm. The positions of the cross sections shown in Figs. 4 and 5 are indicated by broken and dotted vertical lines, respectively. To obtain the subspectra (A) and (B), 110(t_1)* 1024(t_2) complex points were accumulated, with $t_{1,max}(^{13}C)$ = 6.6 ms, $t_{1,max}(^1H)$ = 6.6 ms, and $t_{2,max}(^1H)$ = 184.3 ms. Two scans per increment were acquired and the relaxation delay between scans was set to 1.7 s, resulting in a total measuring time of 26 min. The data matrices were extended to 200 complex points along t_1 by linear prediction (*33*). The digital resolution after zero-filling was 16.2 Hz/pt along $\omega_1(^{13}C/^1H)$ and 2.7 Hz/pt along $\omega_2(^1H)$. (C) Same as (B), except that we used i = 2 and δ = 26.6 ms (Eq. [1] and Fig. 1). Negative peaks are enclosed in circles. A total of 550(t_1)* 1024(t_2) complex points were accumulated, with $t_{1,max}(^{13}C)$ = 33.2 ms, $t_{1,max}(^1H)$ = 33.2 ms, and $t_{2,max}(^1H)$ = 184.3 ms. Two scans per increment were acquired, and the relaxation delay between scans was set to 1.5 s, resulting in a total measuring time of 110 min. The data matrices were extended to 800 complex points along t_1 by linear prediction (*33*). The digital resolution after zero-filling was 4.0 Hz/pt along $\omega_1(^{13}C/^1H)$ and 2.7 Hz/pt along $\omega_2(^1H)$. All spectra were recorded on a Bruker AMX600 spectrometer operating at 600 MHz ^{1}H resonance frequency, which was equipped with a Bruker gradient accessory and a triple-resonance probehead with a self-shielded *z*-gradient coil. Digital filtering was performed with a squared cosine window in t_1 and a sine window shifted by 70° in t_2 (*34*). The spectra were processed and analyzed using the programs PROSA (*35*) and XEASY (*36*), respectively. The chemical shifts are relative to internal tetramethylsilane.

9; note that C′ is decoupled), and those from carbon atoms with none or two carbon coupling partners (for example, C^{β}-MeLeu 9) have opposite signs (Figs. 3C and 5) (*8, 9*).

Multidimensional NMR experiments can be compared in terms of resolution, i.e., the precision of the chemical shift measurement, and in terms of dispersion, i.e., the distribution of peaks encoding chemical shifts in one or several dimensions. Increased resolution may compensate for insufficient dispersion, and vice versa. It is a novel feature of reduced-dimensionality experiments recorded with simultaneous acquisition of central peaks (*5, 15*) that the loss of dispersion arising from the projection can be recovered by symmetrization about the position of the central peaks (Fig. 4). In general, the resolution of a NMR experiment depends on the maximal evolution times, t_{max}, and the transverse relaxation times of the observed nuclei. In constant-time evolution periods the transverse relaxation is manifested by signal attenuation and not by line broadening, so that t_{max} remains as the key variable determining the resolution. The following considerations show that 2D *ct*-HC(C)H-COSY offers significantly increased resolution within a given measurement time when compared with 3D *ct*-HC(C)H-COSY. The spectra in Fig. 3, A and B, were recorded in 26 min with $t_{1,max}$ = 6.6 ms. For identical resolution, the same maximal evolution

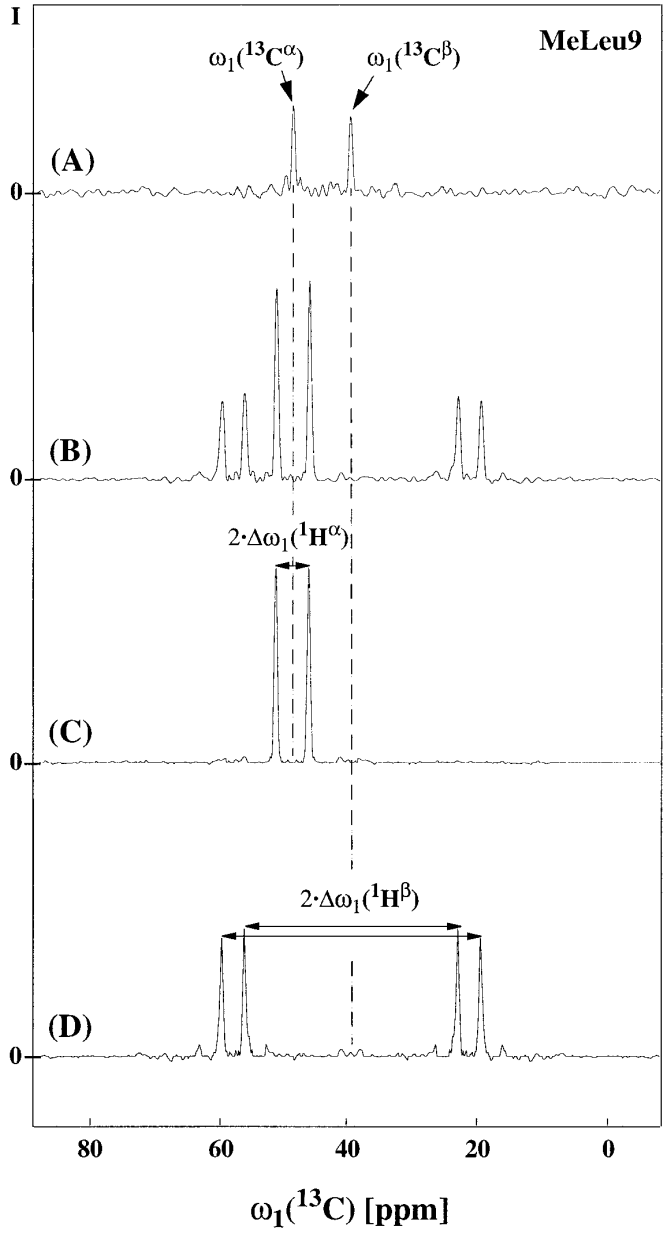

FIG. 4. Cross sections taken along the broken vertical lines from the two subspectra of the 2D *ct*-HC(C)H-COSY experiment in Fig. 3, A and B. The relative intensity, I, is plotted versus the frequency $\omega_1(^{13}C)$. (A) Central peaks detected at $\omega_2(^1H^\alpha)$ of MeLeu9. (B) Peak doublets at $\omega_2(^1H^\alpha)$ of MeLeu9 and $\omega_1(^{13}C^\alpha) \pm \Delta\omega_1(^1H^\alpha)$, and $\omega_1(^{13}C^\beta) \pm \Delta\omega_1(^1H^\beta)$, respectively. (C) and (D) show the spectrum (B) after separation of the C^α and C^β doublets by symmetrization (*16*), which was performed as described in (*5*).

times would have to be achieved for ^1H and ^{13}C in the indirect dimensions of the 3D experiment. Since the ^{13}C dimension can be aliased in the 3D experiment, we assume a corresponding sweep width of 3300 Hz, and the sweep width for the indirect proton dimension shall be 4500 Hz. Then, in 3D HCCH-COSY $t_{1,\max}(^1H) \cdot SW(^1H) = 6.6$ ms $\times$ 4500 Hz $= 30$ complex points must be recorded along $t_1(^1H)$, and $t_{2,\max}(^{13}C) \cdot SW(^{13}C) = 6.6$ ms $\times$ 3300 Hz $=$ 22 complex points must be recorded along $t_2(^{13}C)$. The 2D *ct*-HC(C)H-COSY experiments represent two data sets recorded each with two scans per increment, so that each subspectrum (see Fig. 3, A and B) contains signals which are effectively accumulated with four scans per real increment. However, without symmetrization about the central peaks the signal-to-noise ratio obtained in a projected experiment is reduced by a factor $\sqrt{2}$ when compared with the parent 3D experiment (e.g., *15*). Hence, only two scans per real increment are assumed for the hypothetical 3D experiment. With a relaxation delay of 1.7 s, a time for acquisition and duration of the actual pulse sequence of about 300 ms, and two scans per real increment, we then obtain a measurement time of about 3 hours for the 3D experiment. The same calculation performed for the 2D experiment which was recorded with $t_{1,\max} = 33.2$ ms in 110 min (Fig. 3C) reveals that a hypothetical 3D spectrum sampling both indirect dimensions with $t_{\max} = 33.2$ ms would require about 3 days

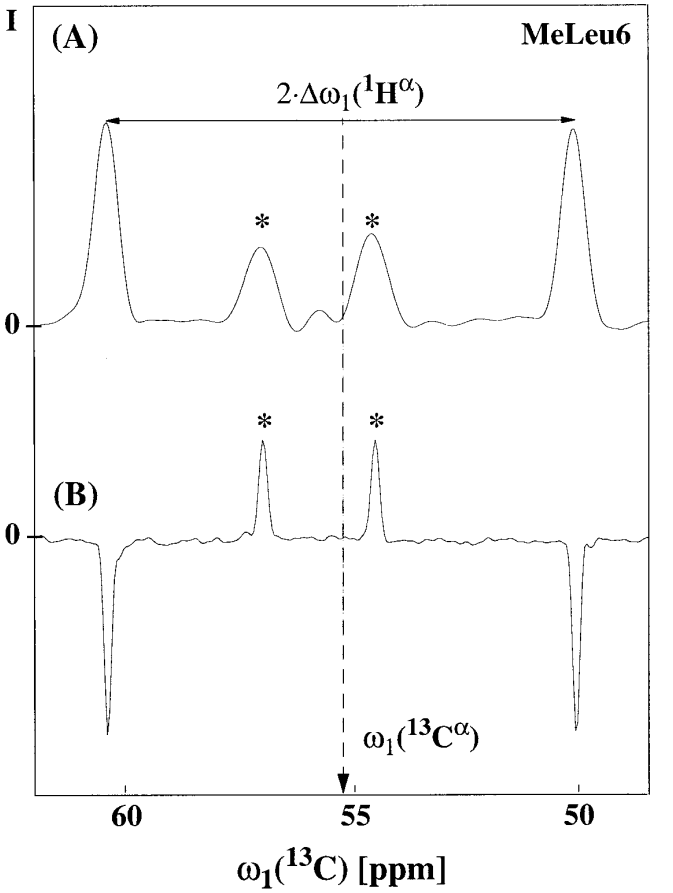

FIG. 5. Cross sections taken along the dotted vertical lines from the 2D *ct*-HC(C)H-COSY subspectra in Fig. 3, B and C. These cross sections contain the doublets detected at $\omega_2(^1H^\alpha)$ of MeLeu6. (A) From Fig. 3B ($t_{1,\max} = 6.6$ ms). (B) From Fig. 3C ($t_{1,\max} = 33.2$ ms). The peaks marked with an asterisk correspond to one component each of the two doublets arising from the nondegenerate β protons of MeLeu6 (in Fig. 3, B and C, all four H^β components are shown).

of instrument time. In view of the high signal-to-noise ratio achieved in the 2D spectra (Figs. 4 and 5) we conclude that the demand of instrument time for the 3D experiment exceeds that dictated by the experimental sensitivity by about two orders of magnitude. The two 3D experiments with t_{max} = 6.6 and 33.2 ms would also represent formidable data sets of 27.5 and 678 MBytes, respectively, which is about 15 and 78 times larger than the data sets acquired for the corresponding projected 2D spectra.

In conclusion, the present experiments demonstrate that 2D *ct*-HC(C)H-COSY can efficiently provide proton and carbon assignments for ^{13}C-labeled low molecular weight biomolecules, which may be studied either free in solution or when bound to a macromolecule. The long transverse ^{13}C relaxation times of small molecules in solution can be exploited to record highly resolved spectra with measurement times that hardly exceed minimal sensitivity requirements. When the ^{13}C-labeled biomolecule is part of a larger macromolecular assembly (up to about 30 kDa), a 2D *ct*-HC(C)H-COSY experiment with $t_{1,max} \approx 1/\{4\,^1J(^{13}C, ^{13}C)\}$ is recommended, since the sensitivity is then comparable to that of the parent 3D experiment, which has successfully been used for large proteins (*18*). In such experiments the heteronuclear pulse scheme of Fig. 1 acts also as a filter for spectral editing when studying a ^{13}C-labeled ligand bound to an unlabeled macromolecule (e.g., *19, 20*). Uniform ^{13}C labeling is obtained ever more efficiently for a variety of compounds, including oligonucleotides (*21, 22*) and oligosaccharides (*23, 24*), so that the 2D *ct*-HC(C)H-COSY experiment should be a viable alternative for a wide range of applications. This includes also resonance assignment and elucidation of the covalent structure and/or the biosynthetic origin of biosynthetically directed fractionally ^{13}C-labeled metabolites (*25–27*). Here, to avoid cancellation of signals arising from different isotopomers, the variant II 2D *ct*-HC(C)H-COSY experiment would be the preferred choice, since such metabolites are in general represented by a pool of isotopomers with different numbers of passive $^1J_{CC}$ couplings.

ACKNOWLEDGMENTS

Financial support was obtained from the Schweizerischer Nationalfonds (Project 31.32033.91) and through a fellowship to C.F. from the ''Schweizerische Bundesstipendienkommission.'' We thank Mrs. R. Hug for the careful processing of the manuscript.

REFERENCES

1. T. Szyperski, G. Wider, J. H. Bushweller, and K. Wüthrich, *J. Biomol. NMR* **3,** 127 (1993).
2. T. Szyperski, G. Wider, J. H. Bushweller, and K. Wüthrich, *J. Am. Chem. Soc.* **115,** 9307 (1993).
3. T. Szyperski, M. Pellecchia, and K. Wüthrich, *J. Magn. Reson. B* **105,** 188 (1994).
4. B. Brutscher, J. P. Simorre, M. S. Caffrey, and D. Marion, *J. Magn. Reson. B* **105,** 77 (1994).
5. T. Szyperski, D. Braun, B. Banecki, and K. Wüthrich, *J. Am. Chem. Soc.* **118,** 4146 (1996).
6. M. Ikura, L. E. Kay, and A. Bax, *J. Biomol. NMR* **1,** 299 (1991).
7. L. Yu, R. Goldman, P. Sullivan, G. F. Walker, and S. W. Fesik, *J. Biomol. NMR* **3,** 429 (1993).
8. G. W. Vuister and A. Bax, *J. Magn. Reson.* **98,** 428 (1992).
9. J. Santoro and G. C. King, *J. Magn. Reson.* **97,** 202 (1992).
10. A. S. Edison, F. Abildgaard, W. M. Westler, E. S. Mooberry, and J. Markley, *Meth. Enzymol.* **239,** 3 (1994).
11. D. P. Burum and R. R. Ernst, *J. Magn. Reson.* **39,** 163 (1980).
12. A. Bax and S. Pochapsky, *J. Magn. Reson.* **99,** 638 (1992).
13. G. Wider and K. Wüthrich, *J. Magn. Reson. B* **102,** 239 (1993).
14. D. Marion and K. Wüthrich, *Biochem. Biophys. Res. Commun.* **113,** 967 (1983).
15. T. Szyperski, D. Braun, C. Fernández, C. Bartels, and K. Wüthrich, *J. Magn. Reson. B* **108,** 197 (1995).
16. R. Baumann, Anil-Kumar, R. R. Ernst, and K. Wüthrich, *J. Magn. Reson.* **44,** 76.
17. H. Kessler, H. R. Loosli, and H. Oschkinat, *Helv. Chim. Acta* **68,** 661 (1985).
18. W. A. Hendrickson and K. Wüthrich (Eds.) ''Macromolecular Structures 1996,'' Current Biology, London, 1994.
19. G. Wider, C. Weber, and K. Wüthrich, *J. Am. Chem. Soc.* **113,** 4676 (1991).
20. D. Lassen, C. Lücke, M. Kveder, A. Mesgarzadeh, J. M. Schmidt, B. Specht, A. Lezius, F. Spener, and H. Rüterjans, *Eur. J. Biochem.* **230,** 266 (1995).
21. E. P. Nikonowicz and A. Pardi, *Nature* **335,** 184 (1992).
22. A. Ono, S. Tate, Y. Ishido, and M. Kainosho, *J. Biomol. NMR* **4,** 581 (1994).
23. C. T. Weller, M. Conville, and S. W. Homans, *Biopolymers* **34,** 1155 (1994).
24. R. Harris, T. J. Rutherford, M. J. Milton, and S. W. Homans, *J. Biomol. NMR* **9,** 47 (1997).
25. R. M. Horak, P. S. Steyn, and R. Vleggar, *Magn. Reson. Chem.* **23,** 995 (1985).
26. H. Senn, B. Braun, B. A. Messerle, C. Weber, R. Traber, and K. Wüthrich, *FEBS Lett.* **249,** 113 (1989).
27. T. Szyperski, D. Neri, B. Leiting, G. Otting, and K. Wüthrich, *J. Biomol. NMR* **2,** 323 (1992).
28. M. H. Levitt and R. Freeman, *J. Magn. Reson.* **33,** 473 (1979).
29. A. Bax, G. M. Clore, P. C. Driscoll, A. M. Gronenborn, M. Ikura, and L. E. Kay, *J. Magn. Reson.* **87,** 620 (1990).
30. A. J. Shaka, C. J. Lee, and A. J. Pines, *J. Magn. Reson.* **77,** 274 (1988).
31. A. J. Shaka, P. B. Barker, and R. Freeman, *J. Magn. Reson.* **64,** 547 (1985).
32. D. Marion, K. Ikura, R. Tschudin, and A. Bax, *J. Magn. Reson.* **85,** 393 (1989).
33. D. S. Stephenson, *Prog. NMR Spectrosc.* **20,** 515 (1988).
34. A. DeMarco and K. Wüthrich, *J. Magn. Reson.* **24,** 201 (1976).
35. P. Güntert, V. Dötsch, G. Wider, and K. Wüthrich, *J. Biomol. NMR* **2,** 619 (1992).
36. C. Bartels, T. H. Xia, M. Billeter, P. Güntert, and K. Wüthrich, *J. Biomol. NMR* **6,** 1 (1995).